TÜBİTAK

Turkish Journal of Earth Sciences

http://journals.tubitak.gov.tr/earth/

Research Article

Turkish J Earth Sci
(2023) 32: 181-199
© TÜBİTAK
doi:10.55730/1300-0985.1837

Deciphering the magma storage conditions and preeruptive processes at Cumaçay: a Plio-Quaternary volcanic eruption center in Eastern Anatolia, Turkey

Yavuz ÖZDEMİR[1,*], **Ayhan ÖZDEMİR**[2]

[1]Department of Geological Engineering, Van-Yüzüncü Yıl University, Van, Turkey
[2]Institute of Natural and Applied Sciences Van-Yüzüncü Yıl University, Van, Turkey

Received: 23.11.2022 • **Accepted/Published Online:** 18.01.2023 • **Final Version:** 27.03.2023

Abstract: We investigate the geology and petrology of Cumaçay, one of the Plio-Quaternary eruption centers of postcollisional volcanism in Eastern Turkey, using a combination of geochronology, bulk-rock geochemistry, thermobarometry, and thermodynamic simulations. Our new K-Ar ages reveal an age of 3.5–0.97 Ma for the eruptive products, which spread around an area of approximately 1000 km^2. Mineral-melt equilibria for olivine, orthopyroxene, clinopyroxene, and plagioclase allow estimation of crystallization pressures, and temperatures indicate two separate crustal storage of crystallization at 14–28 km and 5–15 km. The temperature estimation from diverse methods ranges from 954 °C to 1224 °C. Thermodynamic modelings using Magma Chamber Simulator (MCS) at a representative pressure (5 kbar) imply that the assimilation and crustal contamination (AFC) resulted in evolved melts with various SiO_2 contents at mid to lower crustal depths. Calculated wide range of temperatures, compositional variety from evolved members, and MCS recharge simulation at a representative pressure (2.5 kbar) reveal that the magma mixing between contrasted melts characterizes the final chemical dispersal of the erupted lavas.

Key words: Eastern Anatolia, magma plumbing system, thermobarometry, mineral chemistry

1. Introduction

Reconstructing the magma storage conditions at deep and shallow crustal depths and their petrological evolution is one of the aims of igneous petrology. It is critical to understanding and monitoring future eruption scenarios (e.g., Mcnutt, 2005; White and McCausland, 2016; Cashman et al., 2017). Besides geophysical investigations of fossil and active magma storage regions, petrologic studies of erupted products provide valuable information about magma storage and ascent dynamics. For example, minerals can monitor the whole range of crystallization temperature, pressure, and composition of magma in which they developed during storage and ascent (e.g., Eskandari et al., 2018). This approach has been applied to various intracontinental volcanic regions. Eastern Anatolia is represented by basaltic to rhyolitic lava flows, pyroclastic deposits of postcollisional magmatism extending from the Middle Miocene to historical times (e.g., Keskin et al., 1998; Keskin, 2003; Özdemir et al., 2016, 2019, 2022; Açlan and Altun, 2018; Oyan, 2018). The voluminous postcollisional volcanic activity that erupted from various eruption centers has covered the region and formed extensive basaltic plateaus and active-dormant volcanoes (Pearce et al., 1990; Yılmaz et al., 1998; Keskin, 2003, 2007; Karaoğlu et al., 2005; Özdemir et al., 2006, 2019, 2022; Lebedev et al., 2010, 2016; Özdemir and Güleç, 2014; Oyan et al., 2016, 2017; Açlan et al., 2020). The volume and rock type of the volcanics show variations in time. The Middle Miocene and Quaternary are dominated by intermediate to acidic eruptions; however, the Late Miocene, Pliocene, and Early Quaternary are rich in basaltic products (Özdemir et al., 2022). With the exceptions of limited studies on the magma storage conditions of individual volcanic centers (e.g., Özdemir et al., 2011, 2022; Macdonald et al., 2015; Karaoğlu et al., 2017) previous works on the eastern Anatolian volcanics are mainly concerned with the mantle source region, time-space distribution, and connection with the previous subduction and collision events. Our study focuses on Cumaçay, one of eastern Anatolia's poorly known eruption centers. We report detailed investigations of various ranges of lava types with new K-Ar ages. A combination of whole-rock, mineral chemistry, and thermodynamic simulations is used to reveal magma storage conditions and chemical variations of the Cumaçay.

* Correspondence: yozdemir@yyu.edu.tr

2. Analytical methods

The whole rock geochemistry of the Cumaçay volcanics was determined by ICP-ES and ICP-MS following lithium metaborate/tetraborate fusion and dilute nitric acid digestion at Acme Analytical Laboratories in Canada. Mineral major element compositions were obtained using a CAMECA SX-100 five-wavelength spectrometer (WDS) instrument at the University of Bristol. Minerals were analyzed using a 10 nA beam current, 5 μm beam diameter, and a 20 kV accelerating voltage. Sr and Nd isotopic compositions were conducted at the Pacific Centre for Isotopic and Geochemical Research (PCIGR) at the University of British Columbia. The results of Sr and Nd isotopes were determined on a Thermo-Finnigan Triton TIMS and a Nu Plasma MC-ICP-MS, respectively, using the procedure of Weis et al. (2006). K-Ar age determinations were carried out at the isotope laboratory of IGEM-RAS, Moscow. The radiogenic ^{40}Ar analysis was obtained by the isotope dilution method with mono-isotope ^{38}Ar as a spike on the mass spectrometer MI-1201 IG (SELMI). The precision of the results was controlled by measurements of isotopic compositions of atmospheric argon. FBA-01 spectrometer was used to acquire potassium content in the samples.

3. Results

3.1. Geology and age of the Cumaçay volcanics

Cumaçay volcanics are one of the constituents of eastern Anatolian postcollisional volcanism, exposed 50 km northwest of Ağrı city, covering an area of more than 1000 km^2 (Figure 1). Active right-lateral strike-slip Balık Göl fault cuts across the products of volcanism from the northwest toward the southeast (Sağlam-Selçuk et al., 2021). They cover the Lower Paleozoic metamorphic rocks (Topuz et al., 2017, 2021), allochthonous Late Cretaceous Neotethyan ophiolites/mélanges (Kağızman Complex), Paleocene to Miocene sedimentary rocks and Upper Miocene pyroclastics and intermediate volcanics (Keskin, 1992). The Cumaçay volcanics were first named by Kıral and Çağlayan (1980) and are mainly composed of basalt to rhyolitic lava flows and intermediate to acidic pyroclastic rocks. They are exposed in extensive areas; however, the best outcrops are primarily located around the Cumaçay village (Ergen and Sümengen, 2018). The current study mainly focused on the basaltic, intermediate, and acidic lava members exposed around the Cumaçay village. Our new K-Ar isotopic ages indicate that the Cumaçay volcanics erupted between Upper Pliocene to Pleistocene (Supplementary File 1). The volcanism started with basaltic lava flow, evolved to intermediate and acidic members, and ended with eruption of younger basaltic lava flows. The observed initial product of Cumaçay is a porphyritic basaltic lava flow, exposed northern parts of the study area, flows over the basement strata, and mostly covered by younger basic and intermediate members of the volcanism. A single K-Ar age yields 3.5 ± 0.18 Ma. Following the basaltic lava flow, various lava compositions including basaltic trachyandesites, basaltic andesites,

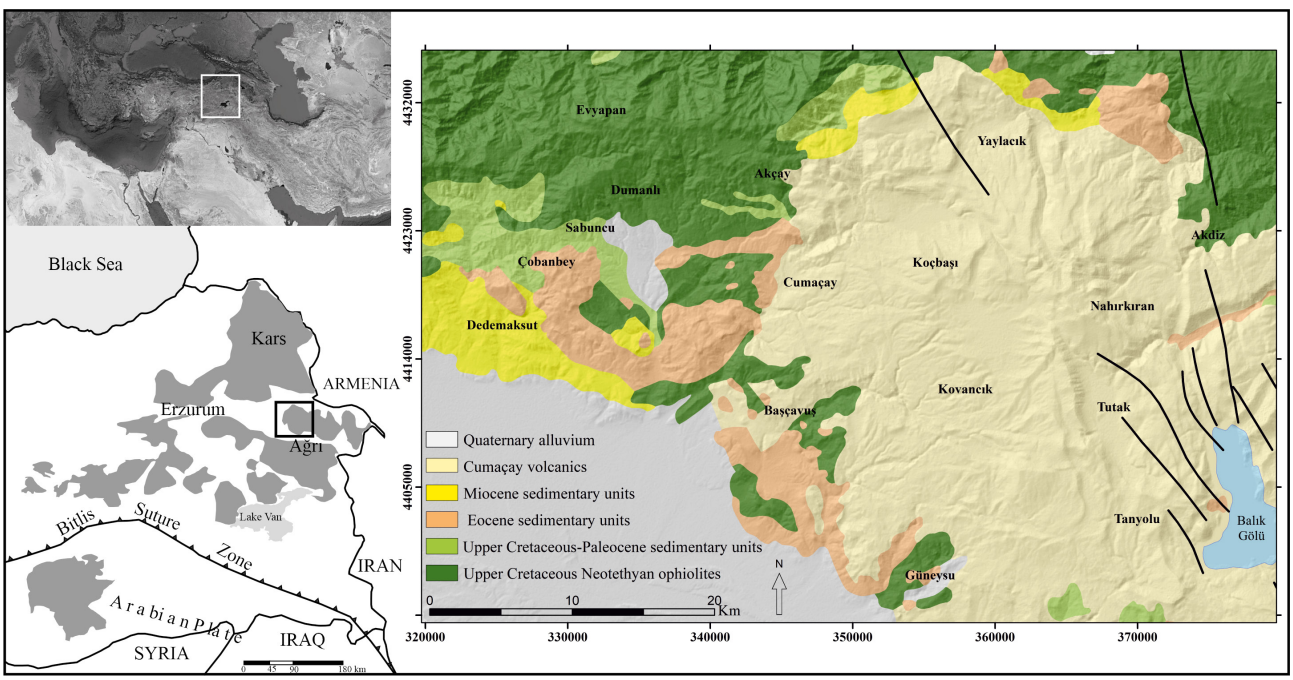

Figure 1. Location (revised from Özdemir et al., 2022) and simplified geological map of the studied area (revised from 1/100,000-scale sheets of the geological map of Turkey, General Directorate for Mineral Research and Exploration).

trachyandesites, andesites, and dacites have erupted. The basaltic trachyandesites and basaltic andesites display porphyritic and glassy textures. K-Ar ages of those lavas are 2.4 ± 0.1 and 2.4 ± 0.12 Ma. Andesites (including trachyandesites) are the most widespread lava flows within the Cumaçay volcanics. Obtained K-Ar ages from the three samples are between 2.9 ± 0.2 and 2.16 ± 0.16 Ma. They are generally porphyritic, occupy high topographies, and mostly overlie the older basaltic and basaltic trachyandesitic lavas. Dacitic lavas have an aphyric texture and cover the andesitic lavas in the southern and northern parts of the study area. The obtained single K-Ar age is 2.1 ± 0.15 Ma. Cumaçay volcanism has ended up with the eruption of two basaltic lava flows. One of them is exposed mainly to northern parts as thick layers, forms columnar jointing, and covers the intermediate and acidic members of the Cumaçay. We obtained a single K-Ar isotopic age of 2 ± 0.2 Ma. The last basaltic flow is the youngest lava flow among all Cumaçay volcanics and is exposed in the southern parts. It is an aphanitic basalt with a K-Ar age of 0.97 ± 0.1 Ma (Supplementary File 1).

3.2. Whole rock and isotope geochemistry

Seventy-two rock samples from Cumaçay volcanics were analyzed for major and trace element compositions. The majority of the samples have low LOI values (<1 wt%), suggesting that the rocks are fresh (Supplementary File 1). Major element compositions (on a hydrous basis) range between 49.25 and 64.62 wt% for SiO_2 and 1.43–7.43 wt% for MgO. Cumaçay volcanics show a compositional spectrum from basalts to dacites (Figure 2). Volcanism started with the mildly alkaline basaltic lava flows, continued with subalkaline intermediate to acidic members, and ended up with transitional and subalkaline basaltic flows. The transitional and subalkaline members are calc-alkaline (Figure 2), and the high Na_2O/K_2O indicates their sodic nature. On conventional Harker diagrams (Figure 3), CaO/Al_2O_3, Fe_2O_3, TiO_2, MgO, Sc, Ni, and Co display negative, but K_2O and total alkalis define negative correlations with SiO_2. The good correlations of selected major and trace element contents would appear to reflect the continuous effect of the chemical differentiation at Cumaçay volcanism. MORB-normalized trace element and chondrite-normalized REE distributions of selected Cumaçay volcanics are given in Figure 4. Large ion lithophile elements (LILE) are enriched in all samples compared to the high field strength elements (HFSE). The element enrichment level seems to increase from basalts to dacites. Basaltic andesites, basaltic tracyandesites, andesites, and dacites have negative Pb, P, and Ti contents. All rock groups display depletion of Nb and Ta, indicating inherited subduction components in mantle source or crustal contamination from country rocks en route to the surface. The Cumaçay volcanics show variable enrichment of light rare earth elements (LREE) over heavy rare earth elements (HREEs) with weak negative Eu anomalies increasing andesites to dacites. The extent of enrichment rises slightly with increasing whole-rock SiO_2 contents (e.g., La/Yb_N; 7.3–7.6 for basalts and 7.6–9 for dacites). The medium rare earth element (MREE) to HREE remains mostly flat over this interval displaying slight fractionation in andesites and dacites (e.g., Sm/Yb_N; 1.9–3.2 for andesites and 2.3–3.4 for dacites). $^{87}Sr/^{86}Sr$ and $^{143}Nd/^{144}Nd$ isotopic ratios of the volcanics vary in the range of 0.703616–0.704762 and 0.512878–0.512757 (Supplementary File 1). The basaltic samples display the lowest Sr and highest Nd isotopic compositions; in contrast, the more evolved lavas have more radiogenic values.

3.3. Mineralogy and petrography

The majority of the Cumaçay volcanics are rich in crystals and porphyritic with hyalopilitic groundmass;

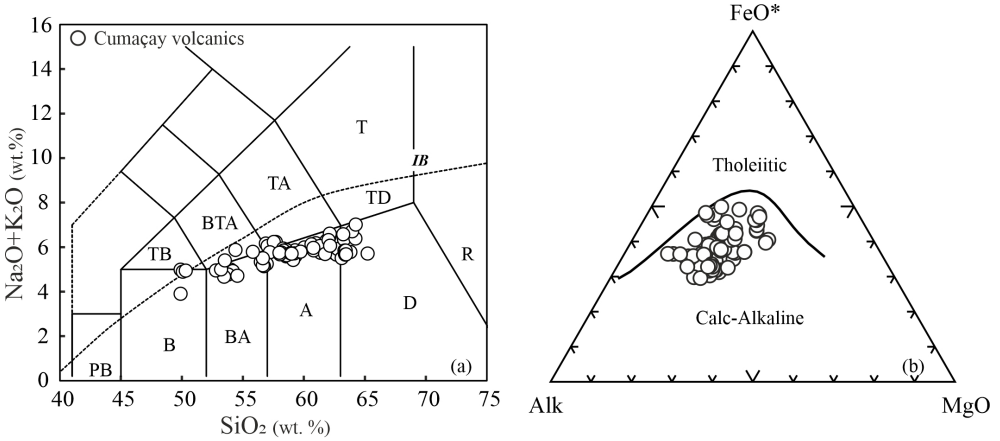

Figure 2. TAS (le Bas et al., 1986) and AFM (Irvine and Baragar, 1971) diagrams for Karayazı-Göksu basalts. The dashed line separating the alkali and subalkaline series (IB) is from Irvine and Baragar (1971).

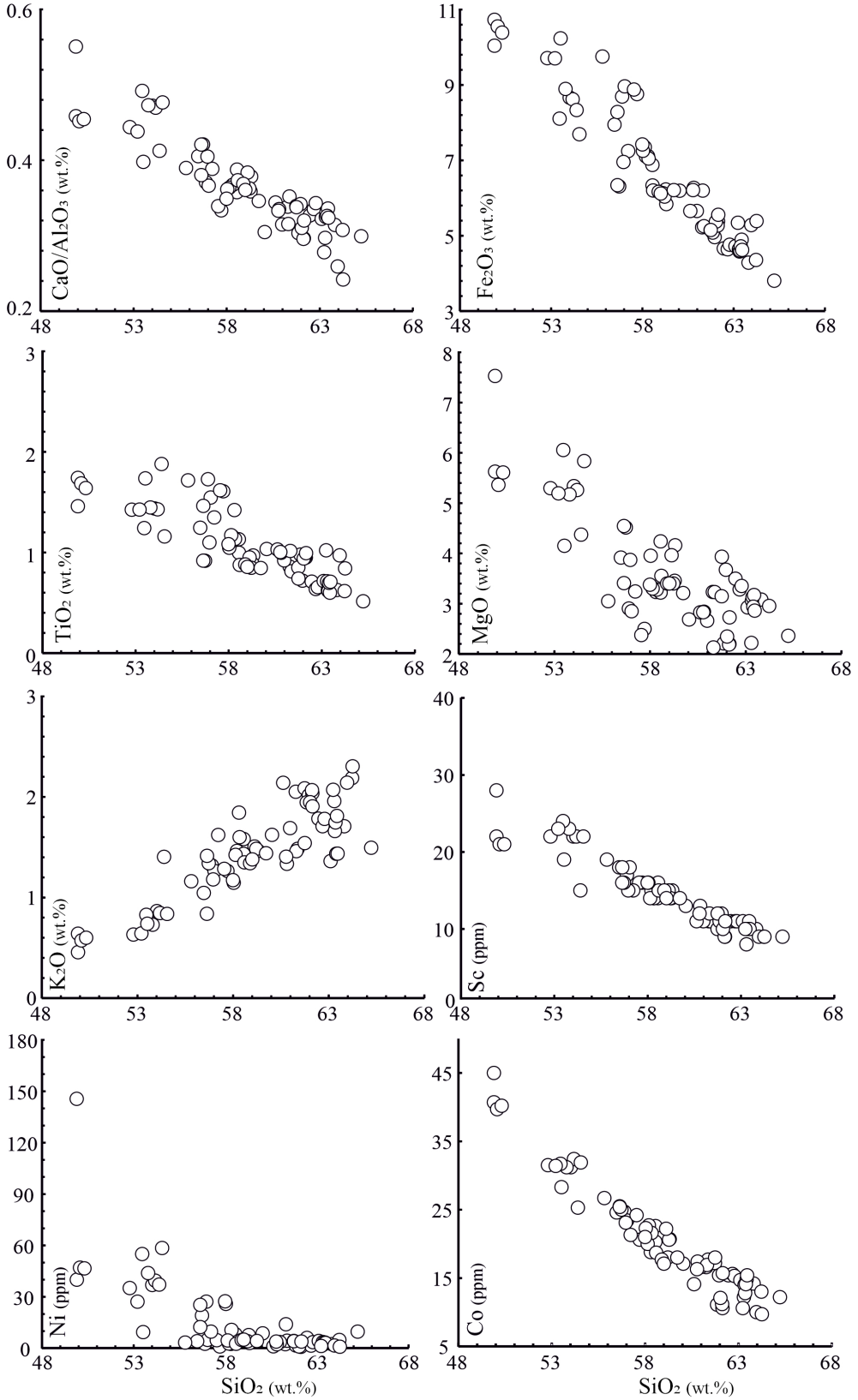

Figure 3. Selected major and trace element variation diagrams of Cumaçay volcanics.

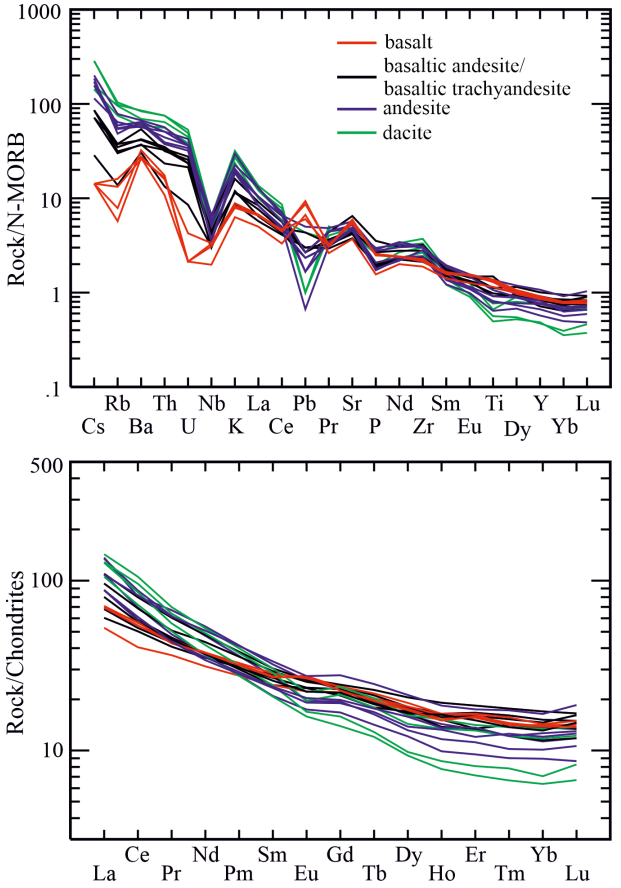

Figure 4. N-MORB normalized multielement and chondrite normalized REE patterns of selected Cumaçay volcanics. Normalization values are from Sun and McDonough (1989).

however, basalts are entirely crystalline. All basaltic lavas contain varying amounts of phenocrysts (>0.5 mm) and microphenocrysts (0.1–0.5 mm) composed of olivine, plagioclase, clinopyroxene, and Fe-Ti oxides. Olivines are in the form of phenocrysts and microphenocrysts with a maximum length of 1.5 mm. They have iddingsite along their rims and display skeletal texture in subalkaline members (Figure 5a). Clinopyroxene is ubiquitous microphenocrysts in all basaltic lava flows. Clinopyroxene and plagioclase display subophitic and glomeroporphyritic textures. Plagioclase phenocrysts are the most common mineral in all basalts, reach up to 1.5 mm in size, and are unzoned or slightly oscillatory zoned. They include melt, pyroxene, and olivine inclusions. Basaltic andesites and basaltic trachyandesites are weakly and highly porphyritic within a fine-grained groundmass. The pyroxenes are common as microphenocrysts. The size of both olivine and plagioclase phenocrysts reaches up to 1.5 mm. Sieve-textured plagioclase crystals have abundant melt and mineral inclusions (e.g., pyroxenes, Figure 5b). The groundmass is crystalline and contains pyroxene, plagioclase, olivine, Fe-Ti oxide microcrystals, and glass. Andesites are texturally highly variable; some are aphyric with feldspar microlites and glassy groundmass, whereas porphyritic ones contain plagioclase, clinopyroxene, orthopyroxene, and Fe-Ti oxides. The size of the plagioclases ranges up to 2 mm; some of them have corroded rims. Othopyroxenes are more abundant than the clinopyroxenes compared to mafic members of the Cumaçay. Dacites are the most evolved members of the Cumaçay volcanism. Some of them are highly vesicular and aphyric with glassy groundmass. The porphyritic examples contain plagioclase, clinopyroxene and orthopyroxene phenocrysts (Figure 5c). The orthopyroxene is the most abundant mafic phase. The amount of clinopyroxene is reduced compared to the intermediate and mafic members. The groundmass contains plagioclase, pyroxene Fe-Ti oxides, and glass. Andesites and dacites are rich in microcrystalline enclaves and crystal clots made of pyroxene, plagioclase, and Fe-Ti oxides (Figure 5d).

3.4. Mineral chemistry

To show the evolution of mineral chemistry with changing the host rock SiO_2 contents, we present analyses as a series of stacked histograms ranked downwards in order of increasing SiO_2 (Figure 6). Mineral chemistry data including one sample each from basalt (Cum175), basaltic trachyandesite (Cum158), andesite (Cum160), and dacite (Cum241), and four samples from basaltic andesites (Cum164;179;181;199) are given in Supplementary File 2.

Olivine

Olivine crystals within different rock groups are normally zoned with forsterite (Fo) rich cores. Fo contents of olivine phenocrysts and microcrystals in basalts range between 81 and 84 (Figure 6a). The Fo of four different basaltic andesites ranges between 68 and 86 mol%. Phenocrysts Fo contents of basaltic andesites decrease with increasing the host rock SiO_2. Olivine microcrystals have the lowest Fo compared with the phenocrysts within the same rock. Some of the olivines with high MgO wt% overlap with the olivine compositions in basalt.

Orthopyroxene

Orthopyroxene is present in basaltic andesite to dacites with increasing abundance. There are scarce pigeonite crystals in these rocks. Orthopyroxenes have a composition range of En_{58-79} and can be classified as enstatite with a 2–4 mol% wollastonite component. As for clinopyroxenes, orthopyroxenes in the basaltic andesites and dacites display relatively limited ranges in Mg# (78–82 and 56–71, respectively), whereas andesite ranges widely between these two extremes (66–81) (Figure 6b). Normally and reversely zoned crystals coexist in andesitic lava.

Clinopyroxene

Clinopyroxenes are Mg-rich augites (En_{37-53}, Fs_{8-23}, Wo_{32-45}) and present in basalts to dacites with decreasing

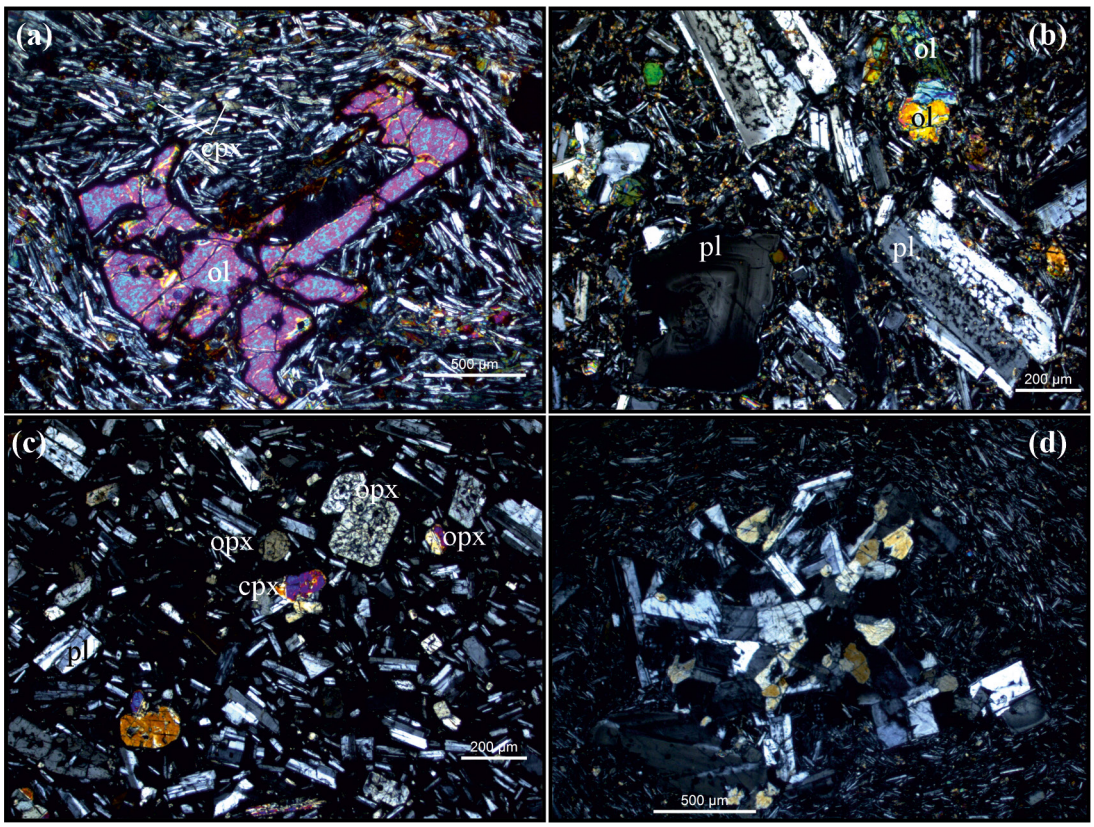

Figure 5. Representative petrographic features of Cumaçay volcanics. a) Skeletal olivine *(ol)* in basalt. b) oscillatory zoned and sieve textured plagioclases *(pl)* in basaltic andesite. c) Orthopyroxene *(opx)* and clinopyroxene *(cpx)* phenocrysts in dacite. d) Pyroxene, plagioclase, and Fe-Ti oxide bearing crystal clot in andesite.

abundance. They occur as microcrystals in basalts, basaltic trachyandesites, and basaltic andesites; however, they form phenocrysts in andesite and dacites. Unzoned, normally, and reversely zoned crystals coexist in the same sample. The Mg# (molar Mg/(Mg+Fe) of clinopyroxenes shows a decrease from mafic to acidic members (Figure 6c). The Mg# of clinopyroxenes in basalt, basaltic andesites, and basaltic trachyandesite is in the range of 69–76, 66–85, and 63–76, respectively. However, Mg# of clinopyroxenes in andesite has a wide compositional range (63–81; Figure 6c). A single clinopyroxene in a dacitic sample yields an Mg# of 63 (not shown).

Plagioclase

Plagioclase is the most abundant phenocryst and occurs in almost every rock sample either as phenocrysts or in the groundmass. The composition of plagioclases ranges from bytownite to andesine. Overall, there is a general decrease in anorthite (An) content with increasing host rock SiO_2. Some of the plagioclase phenocrysts in basalt typically have slightly more An-rich rims than cores. Composition of the plagioclases in basalt is in the range of An_{69-60} (Figure 6d). Plagioclase in basaltic andesites records the highest anorthite contents (An_{48-79}). The lower An contents are typically from the rim or microcrystal compositions. Plagioclases in basaltic trachyandesite have a lower content of An (An_{57-43}) compared to basalts and basaltic andesites (Figure 6d). Normal zoning is dominant with a rimward decrease of only 1–2 mol% An. The An contents of phenocrysts display a wide range in andesite (An_{31-70}) and dacite (An_{37-64}), which is more prominent in andesite.

Fe-Ti oxides

Ilmenite and titanomagnetite are observed in most of the Cumaçay volcanics. They occur as groundmass crystals, inclusions in other phenocrysts, and rarely as phenocrysts. The ulvospinel component in the cores of titanomagnetites ranges from 24 to 66 mol%. Ilmenite contents in ilmenite crystals range from 59 to 96 mol%.

3.5. Conditions of magma storage and eruption

In this section, we report and discuss our results using the various multiple minerals and mineral/liquid methods available in the literature. Intensive magmatic parameters, such as temperature (T), pressure (P), oxygen fugacity (fO_2), and melt water content (H_2O) at preeruptive conditions, could be presented through these models. The results of the different approaches are given in Table 1.

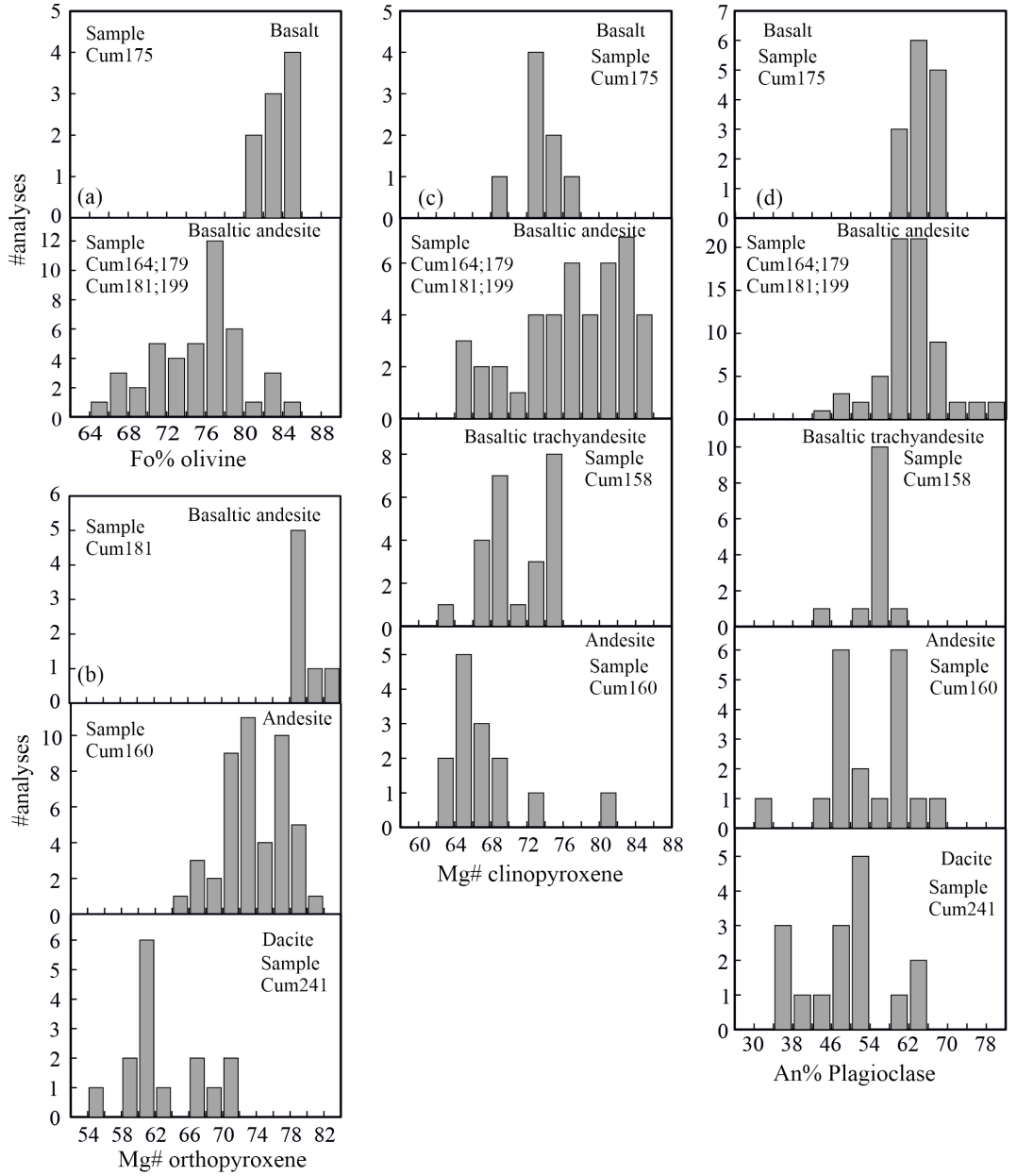

Figure 6. Frequency distribution diagrams for olivine (a), orthopyroxene (b), clinopyroxene (c), and plagioclase (d) grouped based on the host rock composition.

3.5.1. Initial estimates by independent variables

One of the main difficulties of employing the geothermometers is the requirement of some parameters, such as P, H_2O, and T. It is, therefore, crucial that independent methods accurately determine one or more variables (e.g., Polo et al., 2017). For this reason, we first applied Fe-Ti oxide and clinopyroxene-liquid to calculate the temperature and pressures.

Coexisting magnetite-ilmenite pairs are rare in the Cumaçay volcanics, most of which are from groundmass microcrystals. Due to the rarity of the touching oxide pairs, we also used individual crystals within the same thin section for temperature, and oxygen fugacity (fO_2) estimates. Each magnetite was checked against each ilmenite analysis for the same sample to test the Mg/Mn equilibrium (Bacon and Hirschmann, 1988). Only data that passed this test were used for the calculations (Table 1). Suitable pairs were then processed using the method of Anderson and Lindsley (1985), with the recalculation scheme of Stormer (1983) for fO_2 and T estimates (Figure 7a). In basalt, Fe-Ti oxide temperatures range between 1009 and 1090 °C. Temperatures from basaltic andesites

Table 1. Temperature, pressure, and melt H_2O estimated for Cumaçay volcanics (B: basalt, BA: basaltic andesite, BTA: basaltic trachyandesite, A: andesite, D: dacite).

	Temperature (°C)						**Pressure (kbar)**				**H_2Omelt (wt%)**
Sample no.	Stormer (1983) Fe/Ti oxide	Putirka (2003) CPX/liquid	Putirka (2008) CPX/liquid Eq.33	Putirka (2008) OPX/liquid Eq.28a	Putirka (2008) Ol/liquid Eq.22	Putirka (2005) Plag/liquid Eq.23	Putirka (2003) CPX/liquid	Putirka (2008) CPX/liquid Eq.30	Putirka (2008) OPX/liquid Eq.29a	Putirka (2005) Plag/liquid Eq.25a	Waters and Lange (2015)
Cum175 (B)	1009–1090	1166–1187	1117–1153		1211–1224	1203–1207	3.7–6.6	1.3–5.2		6.9–7.8	0.6–0.7
Cum164(BA)	885–987	1121–1132	1094		1152	1141–1146	1.9	2.0		3.7–4.3	1.3–1.6
Cum179(BA)	999	1140–1200	1153–1170		1168	1161–1167	0.9–7.1	5.7–7.6		4.8–6.5	1.2–1.3
Cum181(BA)	842–888	1168–1186	1146–1161	1152–1156	1167–1170	1166–1172	4.8–6.4	5.0–7.2	4	4.8–6.2	0.8–1.1
Cum199(BA)	893–1019				1152–1171	1138–1170				4.4–6.7	0.9–1.1
Cum158(BTA)	857–1016	1050–1116	1042–1111			1081–1087		4.3–4.8		3.2–6.54	2.0–2.2
Cum160(A)		1081–1115	1045	1056–1079		1072–1084		2.5	1.0–3.0	2.8–4.9	1.5–1.9
Cum241(D)	954–967			954–990		964–974			1.0–4.0	1.0–1.4	3.7–4.0

and basaltic trachyandesite yield lower temperatures than the basaltic sample, ranging from 842 to 1019 °C and 848 to 1016 °C, respectively. Fe-Ti oxide crystallization temperatures from the dacite narrowly range between 954 and 967 °C.

The second method applied is the clinopyroxene-liquid thermometer of Putirka et al. (2003), which requires a pressure input and not water content. Pressure input has minimal effect on calculating the crystallization temperatures. Two different equilibrium tests were carried out to apply the clinopyroxene-liquid thermometers; the exchange coefficient between melt and clinopyroxene K_D $(Fe\text{-}Mg)^{cpx\text{-}lig}$ = 0.28 ± 0.08 (Putirka, 2008) and the comparison of the measured clinopyroxene geochemistry with the predicted ones obtained from regression analysis of clinopyroxene-melt pairs. (Figure 7b). The whole-rock composition was assumed to be nominal melt composition in both tests. Only the measured clinopyroxenes that pass both requirements for equilibrium were used for temperature estimates. Clinopyroxene-melt pairs of basaltic rock have crystallization temperatures of 1166–1187 °C. Temperatures from basaltic andesites lie from 1140 to 1200 °C. Basaltic trachyandesite and andesite have crystallization temperature ranges of 1050–1116 °C and 1081–1115 °C, respectively. The calculated pressures from this method yield 3.7–6.6 kbar for basalt and 0.9–7.1 kbar for basaltic andesites (Table 1).

H_2O contents

The plagioclase–liquid hygrometer of Waters and Lange (2015) was used to calculate the preeruptive melt H_2O contents of Cumaçay volcanics. The method is based on the crystal-liquid exchange reaction between the albite and anorthite components and is temperature-dependent (pressure has a minor effect). Bulk compositions of the rocks are used as the nominal liquid, and selected plagioclase core (an-max) compositions, most likely to be in equilibrium with the bulk rock, are used for the melt water concentrations. Our calculations used pressures and average temperatures from clinopyroxene–liquid (except dacitic sample) methods as P and T inputs. The temperature for a dacitic sample is from the Fe-Ti oxide thermometer. Calculated H_2O contents range from 0.6 to 0.7 wt% for basalt, 0.8 to 1.6 wt% for basaltic andesites, 2.1 to 2.2 wt% for basaltic trachyandesites, 1.6 to 1.9 wt% for andesite, and 3.7 to 4 wt% for dacite (Table 1).

Oxygen fugacity

Oxygen fugacity was defined using the Fe-Ti oxide equilibria following the same method for Fe-Ti oxide thermometry. Each Fe-Ti oxide pair was processed by the method reported by Spencer and Lindsley (1981), with the recalculation scheme of Stormer (1983), and calculated as log units relative to the FMQ buffer (Figure 7a). ΔFMQ values range from –0.9 to 1.77. The lowest fO2 is recorded by basaltic andesite (ΔFMQ: –0.05 to +0.06; Cum181). The highest fO2 is from basaltic trachyandesite (ΔFMQ: 1.21–1.77; Cum158).

3.5.2. Magma temperatures and pressures

Once obtaining the first T-P-H_2O wt%, we can apply other accurate methods to calculate crystallization P and T for Cumaçay volcanics. A summary of the different approaches is given in Table 1. The olivine-liquid (Putirka, 2008), clinopyroxene-liquid (Putirka, 2008), plagioclase-liquid (Putirka, 2005), and orthopyroxene-liquid (Putirka, 2008) geothermometers were used to monitor the crystallization conditions of the Cumaçay volcanics.

Clinopyroxene-liquid

The equilibrium conditions between clinopyroxene and nominal liquid (whole rock composition) are the same as described above. Melt H_2O contents are from the method of Walters and Lange (2015) (Table 1). Equations of 33 and 30 from Putirka (2008) are used to estimate temperature and pressure. Clinopyroxene-melt pairs of basaltic sample produce temperatures of 1117–1153 °C and pressures of 1.3–5.2 kbar. T and P conditions of basaltic andesites lie from 1094 to 1170 °C and 2 to 7.6 kbar, respectively. The basaltic trachyandesite and andesite have relatively lower temperatures ranging from 1042 to 1111 °C. The crystallization pressure of basaltic trachyandesite is in the range of 4.3–4.8 kbar. A single clinopyroxene-melt pair yields a pressure of 2.6 kbar for the andesite.

Orthopyroxene-liquid

Orthopyroxene compositions were evaluated for equilibrium with whole rock compositions based on K_D $(Fe\text{-}Mg)^{opx\text{-}liq}$ = 0.29 ± 0.06 (Putirka, 2008) (Figure 7c). Crystals not in equilibrium with nominal melt are excluded and not considered in interpretations. Equilibrium mineral-melt pairs, the input of melt H_2O contents, and preferred pressures are given in Table 1. Based on the equations of 28a and 29a from Putirka (2008), basaltic andesite, andesite, and dacite have temperatures and pressures of 1152–1156 °C and 4 kbar, 1056–1079 °C and 1–3 kbar, 954–990 °C and 1–4 kbar, respectively.

Olivine-liquid

Olivine-liquid thermometry (Putirka, 2008; Eq.22) was used to calculate the temperatures for basalts and basaltic andesites. The composition of the whole rock is used for the nominal liquid composition. The mineral-liquid equilibria were checked using the method of Roeder and Emslie (1970). The phenocrysts that passed the equilibrium test (K_D $(Fe\text{-}Mg)^{ol\text{-}liq}$ = 0.30 ± 0.03; Figure 7d) are used for temperature estimates. Since the olivine liquid equilibria is sensitive to pressure and water contents, we used calculated melt water contents from Walter and Lange (2015) (Table 1) and maximum pressure (7.6 kbar) from clinopyroxene-liquid equilibria (Table 1). The temperatures obtained from the olivin-liquid thermometer

are in the range of 1211–1224 °C for basalts and 1152–1170 °C for basaltic andesites.

Plagioclase-Liquid

Putirka (2008) proposed that the temperature, pressure, and melt H_2O content have little effect on the Ab-An exchange coefficient. Thus the K_D $(Ab\text{-}An)^{plag\text{-}liq}$ exchange between crystal and melt 0.28 ± 0.11 for T > 1050 °C and 0.1 ± 0.05 < 1050 °C can be used for equilibrium (Putirka, 2008) (Figure 7e). Plagioclase-liquid equilibrium temperatures and pressures are estimated by carrying out equations 23 and 25a from Putirka (2005) using estimated melt H_2O content for each rock group (Table 1). Based on the available plagioclase compositions, water, and pressure data, the plagioclase liquid geothermometer yield a temperature and pressure range of 1203 to 1207 °C and 6.9–7.8 kbar for basalts, 1138–1172 °C and 3.7–6.7 kbar for basaltic andesites, 1081 to 1087 °C and 3.2–6.54 kbar for basaltic trachyandesite, 1072 to 1084 °C and 2.8–4.9 for andesite, and 964 to 974 °C and 1–1.4 kbar for dacite.

Summary of temperature and pressure

Calculated temperatures from diverse methods are broadly consistent with fractionation from basalts (≤1224 °C) to dacites (954 °C) (Figure 8a). Temperatures generally decrease with increasing SiO_2 contents of host rock SiO_2. However, andesite (Cum160) has a nearly similar temperature range to that of the basaltic trachyandesitic

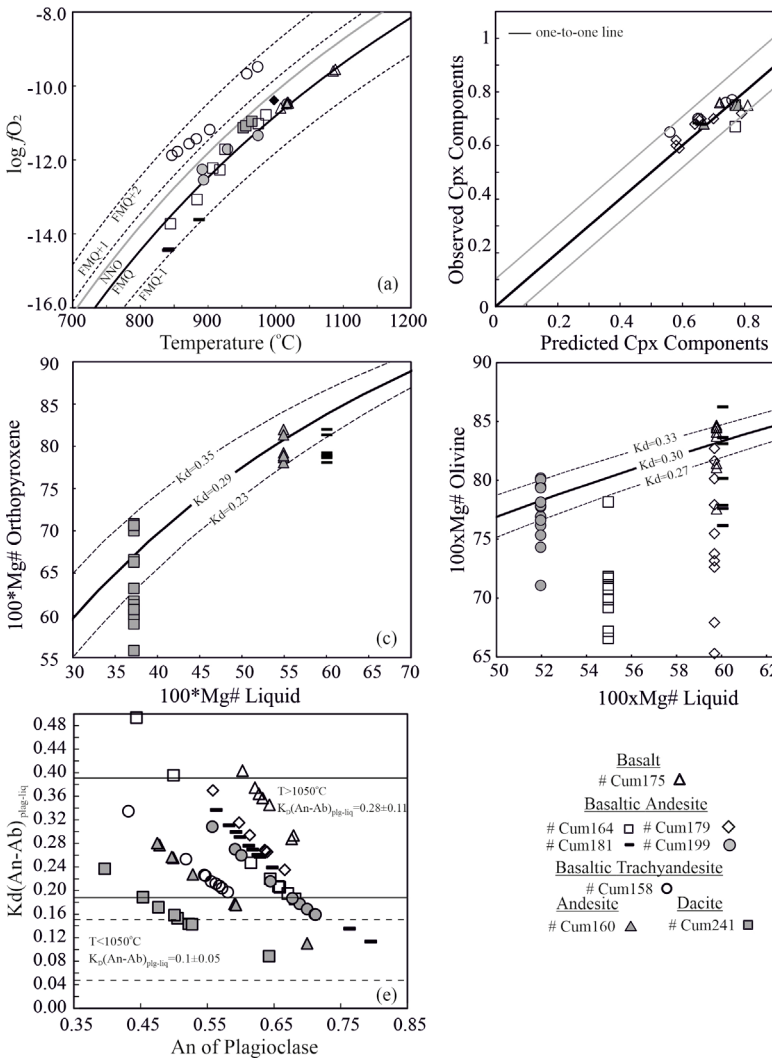

Figure 7. a) Temperature versus oxygen fugacity, calculated from Fe-Ti equilibria using the ILMAT program (Lepage 2003). b) Clinopyroxene-liquid equilibrium test according to observed and predicted (Dihd) compositions (Putirka, 1999). Equilibrium test based on the Fe-Mg exchange reaction between orthopyroxene (c) or olivine (d) and liquid ($^{Fe\text{-}Mg}KD_{opx\text{-}liq}$=0.29 ± 0.06 and $^{Fe\text{-}Mg}KD_{ol\text{-}liq}$=0.30 ± 0.03; Putirka, 2008). e) Plagioclase-liquid equilibrium test for the Ab-An exchange reaction by the model of Putirka (2005, 2008). The stability field was drawn using a value for $^{Ab\text{-}An}KD_{pl\text{-}liq}$ = 0.28 ± 0.11, T > 1050 °C (continuous lines), and $^{Ab\text{-}An}Kd_{pl\text{-}liq}$=0.1 ± 0.05, T < 1050 °C (dotted lines).

lava (Cum158). Olivine-liquid temperatures overlap or are slightly higher than the plagioclase liquid temperatures in basalt and basaltic trachyandesites. Clinopyroxene-liquid temperatures have the lowest values in basalts; however, they mostly match up with the plagioclase-liquid and orthopyroxene-liquid temperatures in basaltic andesites, basaltic trachyandesite, and andesite. Fe-Ti oxide temperatures from diverse rock groups are predominantly from groundmass microcrystals rather than phenocrysts and lower than the other methods (except for dacite) and probably reflect most closely the temperature shortly before the eruption due to their fast reequilibration (Venezky and Rutherford, 1999) or underwent reequilibration upon slow cooling of the lava flow (e.g., Özdemir et al., 2011).

The preeruptive pressures using different thermodynamic barometers vary between approximately 8 kbar and approximately 1 kbar and mostly overlap (Figure 8b). Crystallization pressures from diverse methods for basalt and basaltic andesites mainly clustered between 3.7 and 7.8 kbar. Basaltic trachyandesite displays a wide range of crystallization pressures from 3.2 to 6.5 kbar. Andesite and dacite yield pressures of 1–4.9 and 1–4 kbar, respectively.

4. Discussion

4.1. Assessing magma differentiation processes

Cumaçay volcanics have low ranges of Mg#, Co, and Ni (Supplementary File 1), suggesting they are not primary melts and have undergone fractional crystallization. The covariation diagrams of whole-rock major and trace elements show negative correlations in CaO/Al_2O_3, MgO,

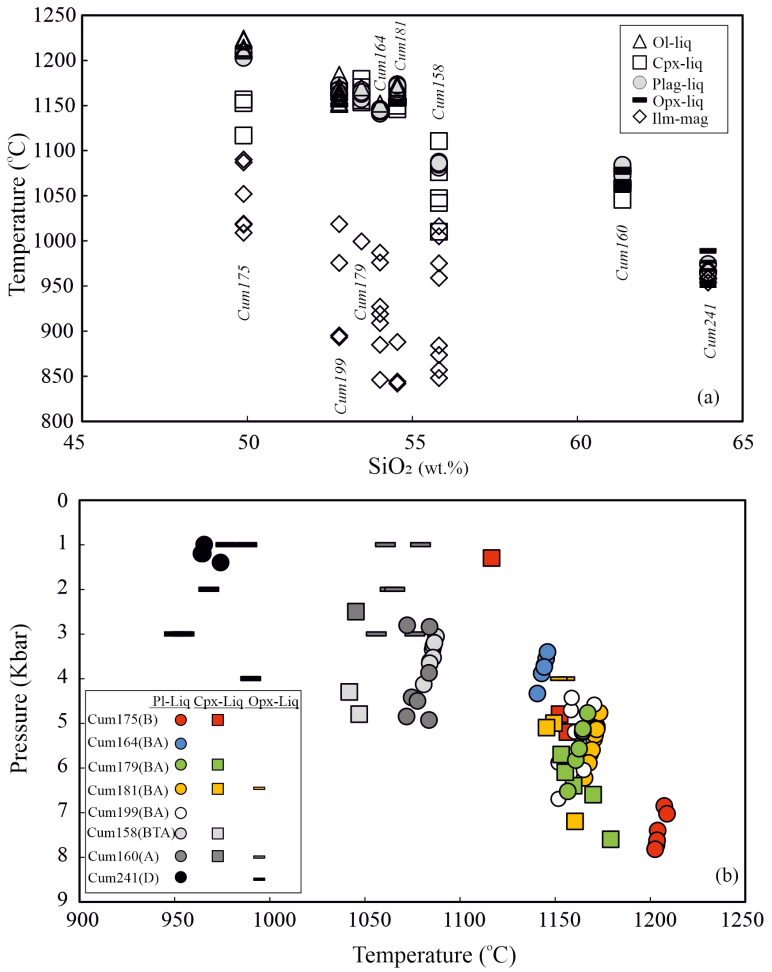

Figure 8. Temperature versus SiO_2 (a) and pressure (b) diagrams for Cumaçay volcanics. Calculation methods are the same as in Table 1. For cpx-liq, only the results of Putirka (2008) are plotted. Key to abbreviations: *A* andesite, *B* basalt, *BA* basaltic andesite, *BTA* basaltic trachyandesite, *D* dacite, *Cpx* clinopyroxene, *Ilm* ilmenite, *Liq* liquid, *Mag* magnetite *Opx* orthopyroxene, *Ol* olivine, *Pl* plagioclase.

Sc, Ni, and Co with increasing content of SiO_2 (Figure 3), indicating crystallization of olivine and pyroxene from their parental melts. Drops in contents of Fe_2O_3 and TiO_2 (Figure 3) with increasing degrees of differentiation are consistent with the fractionation of Fe-Ti oxides that are ubiquitous as microcrystals. The lack of strong negative Eu anomaly in basaltic and intermediate rock indicates an insignificant role of plagioclase. However, a decrease in Sr contents of the rocks with SiO_2 contents > 62 wt% and slightly negative Eu anomaly in REE patterns (Figure 4) suggest the role of plagioclase in dacitic members. The crystallization temperatures obtained from various thermometers also indicate a progressive decrease from basaltic members of Cumaçay towards more fractionated lavas. However, the $^{87}Sr/^{86}Sr$ and $^{143}Nd/^{144}Nd$, isotopic compositions of the Cumaçay volcanics vary systematically with SiO_2 contents. Positive correlations between $^{87}Sr/^{86}Sr$ and SiO_2 and negative correlation between $^{143}Nd/^{144}N$ and SiO_2 (Figure 9) could not be explained solely by closed system fractionation; instead, they suggest that Cumaçay volcanics produced in an open system through assimilation and fractional crystallization and/or magma mixing.

The results of thermobarometry (Figure 8b) suggest two crustal magma reservoirs beneath Cumaçay: (1) a deep magma reservoir at crustal pressures between approximately 4–7.8 kbar (mainly clustered at 5–6 kbar) where primitive basaltic magmas undergone fractional crystallization and/or assimilation processes (2) a shallow magma chamber at crustal pressures of 1.5–4.5 kbar (mainly clustered at 2–3 kbar) where ascending evolved magmas from deeper reservoir settled into and undergone fractional crystallization and/or magma mixing (recharge). In order to discuss these two possible petrological processes, the recently developed Magma Chamber Simulator (MCS) program (Bohrson et al., 2014; 2020) has been used for thermodynamic modeling based on major element compositions of Cumaçay volcanics. MCS uses rhyolite MELTS (Ghiorso and Sack, 1995; Gualda et al., 2012; Ghiorso and Gualda, 2015) as its thermodynamic engine and simulates the thermodynamic and geochemical evolution of an isobaric multicomponent-multiphase open magma system. The input for MCS models covers major element composition, pressure, temperature, and mass constraints for parental magmas and wall rock (Bohrson et al., 2014; 2020). In order to model fractional crystallization (FC) and assimilation and fractional crystallization (AFC) processes in a deep magma reservoir, we have used a basaltic sample (Cum175, Table 2) as parental magma composition with the lowest $^{87}Sr/^{86}Sr$ and the highest $^{143}Nd/^{144}Nd$ and MgO contents within the whole Cumaçay volcanics. We employed 0.5 wt% H_2O and 1wt% H_2O as initial water concentrations to parental magma composition following the values obtained from plagioclase–liquid hygrometer (Table 1). Bulk composition of Paleozoic schist was used as wall rock composition in AFC models. The initial wall rock temperature was taken as 700 °C giving a geothermal gradient of approximately 39 °C/km higher than the average crustal geothermal gradient of approximately 28 °C/km, assuming that the previous magma injections to the crust have already heated the wall rock. To evaluate the effects of fO2 on our evolving magma and wall rock, we conducted our models at FMQ, FMQ+1, and FMQ+2 buffers. We performed models for the deep magma reservoir at 5 kbar (approximately 18 km, assuming a crustal density of 2800 kg/cm^3) corresponding to the main magma pressures obtained from mineral-mineral and mineral liquid equilibria (Figure 8b). For a shallow magma reservoir, we carried out a recharge and fractional crystallization modeling (RFC) at 2.5 kbar (approximately 9 km) using dacite (#Cum238) as resident magma and a basaltic trachyandesite (#Cum179) (Table 2) for recharge magma. The recharge event of 75 mass units (m.u.) is introduced at approximately 1046 °C. Fe^{2+}/Fe^t ratios relative to the buffers at the model pressures are calculated using the MELTS-excell interface (Gualda and Ghiorso, 2015).

4.1.1. Fractional crystallization (FC) models

The crystallinity of the Cumaçay magmas is decreasing from runs at FMQ to FMQ+2, ranging between 90% and 79%. FC models predict crystallization of orthopyroxene (approximately 3–12 wt%), clinopyroxene (19–31wt%), pigeonite (8–16wt%), plagioclase (approximately 45–52wt%), Fe-Ti oxide (approximately 7–11wt%) and minor amounts of apatite. None of the runs predicts olivine crystallization which is one of the mafic mineral phases in mafic members of Cumaçay. Pigeonite, which is rarely observed in natural rocks, only stabilized at FMQ and FMQ +1 runs with 0.5 wt% H_2O. The liquid lines of descent (LLD) modeled by MSC, along with the Cumaçay volcanics, are given in Figure 10. They do not fully reproduce the whole rock compositions of natural products. Modeled curves at FMQ+1 and FMQ+2 with 1wt% H_2O replicate some of the basaltic andesites, basaltic trachyandesites, andesites, and dacites of the Cumaçay volcanics for MgO, CaO, and FeO. However, it fails for more felsic members for Al_2O_3 and total alkalis (Na_2O+K_2O). Runs at FMQ (0.5–1 wt% H_2O) and FMQ+1 (0.5 wt% H_2O) predict high Na_2O+K_2O and alkaline character towards the higher SiO_2 contents. Runs at FMQ+1 (1 wt% H_2O) and FMQ+2 (0.5–1 wt% H_2O) reproduced Cumaçay volcanics from approximately 50 to approximately 58 wt% SiO_2 and simulated higher Na_2O+K_2O towards the evolved compositions

4.1.2. Assimilation and fractional crystallization (AFC) models

The striking feature of the Cumaçay volcanics are variations of the isotopic compositions towards more

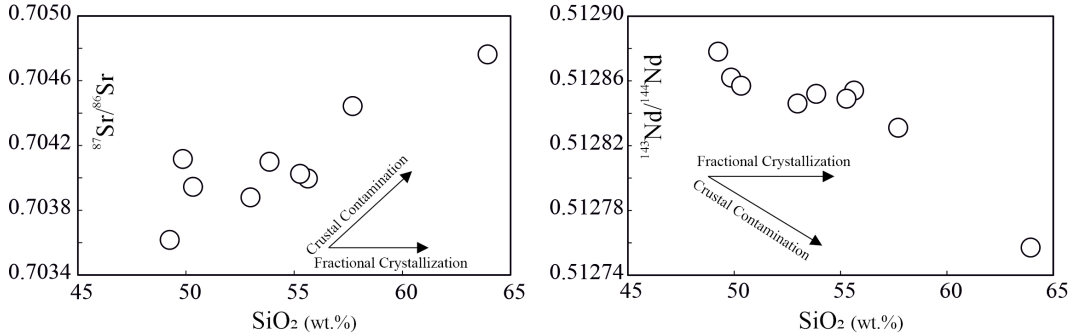

Figure 9. SiO_2 versus $^{87}Sr/^{86}Sr$ and $^{143}Nd/^{144}Nd$ diagrams for Cumaçay volcanics.

Table 2. Parental melt (M), wall rock (WR), and recharge (R) compositions and parameters used in FC, AFC, and RFC runs*.

	FC and AFC		**RFC**	
	M (Cum175)	**WR (CMK13)**	**M (#Cum238)**	**R (Cum179)**
SiO_2(%)	49.90	54.99	64.23	53.47
TiO_2	1.46	1.41	0.61	1.24
Al_2O_3	17.34	16.10	16.26	17.50
Fe_2O_3TOT	10.04	14.16	4.36	8.10
MnO	0.16	0.12	0.07	0.13
MgO	7.53	8.97	2.95	6.06
CaO	9.54	1.42	5.00	8.61
Na_2O	3.44	2.61	4.19	3.83
K_2O	0.46	0.08	2.19	0.83
P_2O_5	0.18	0.14	0.23	0.22
	FC: Melt	Wall rock	AFC: Melt	RFC: Melt
Pressure (kbar)	5	5	5	2.5
Mass (m.u.)	100	100		75
Decrement,ΔT(°C)	10		10	
Initial wall-rock T(°C)		700		
FmZero		0.05		
Initial recharge T(°C)				1200
Recharge trigger T(°C)				1050

*For AFC runs parent magma Fe^{+2}/Fe^{+3} was calculated at FMQ, FMQ+1, and FMQ+2 at liquidus temperatures after adding 0.5–1 wt% H_2O; for WR Fe^{+2}/Fe^{+3} was calculated at FMQ, FMQ+1, and FMQ+2 at 750 °C and at 5 kbar after adding 1 wt% H_2O; for RFC run parent magma Fe^{+2}/Fe^{+3} was calculated at FMQ+2 at liquidus and at 2.5 kbar after adding 4 wt% H_2O.

evolved samples (Figure 9), which could result from contamination from the continental crust. Since FC models fail to reproduce evolved acidic members in Na_2+K_2O and Al_2O_3 space and linear geochemical trends observed in CaO, MgO, and FeO (approximately 54–65 %wt SiO_2) contents, we have performed a series of MCS models to test whether the assimilation of wall rock melt during fractional crystallization could overcome these problems. We chose the same basalt (Cum175) that we used in FC models as parental magma composition, and Paleozoic schist (CMK13) represents the continental crust (wall rock composition) of the region (Table 2). Modeled major element compositions are given in Figure 11. Total anatectic melt assimilated by magma range between 22

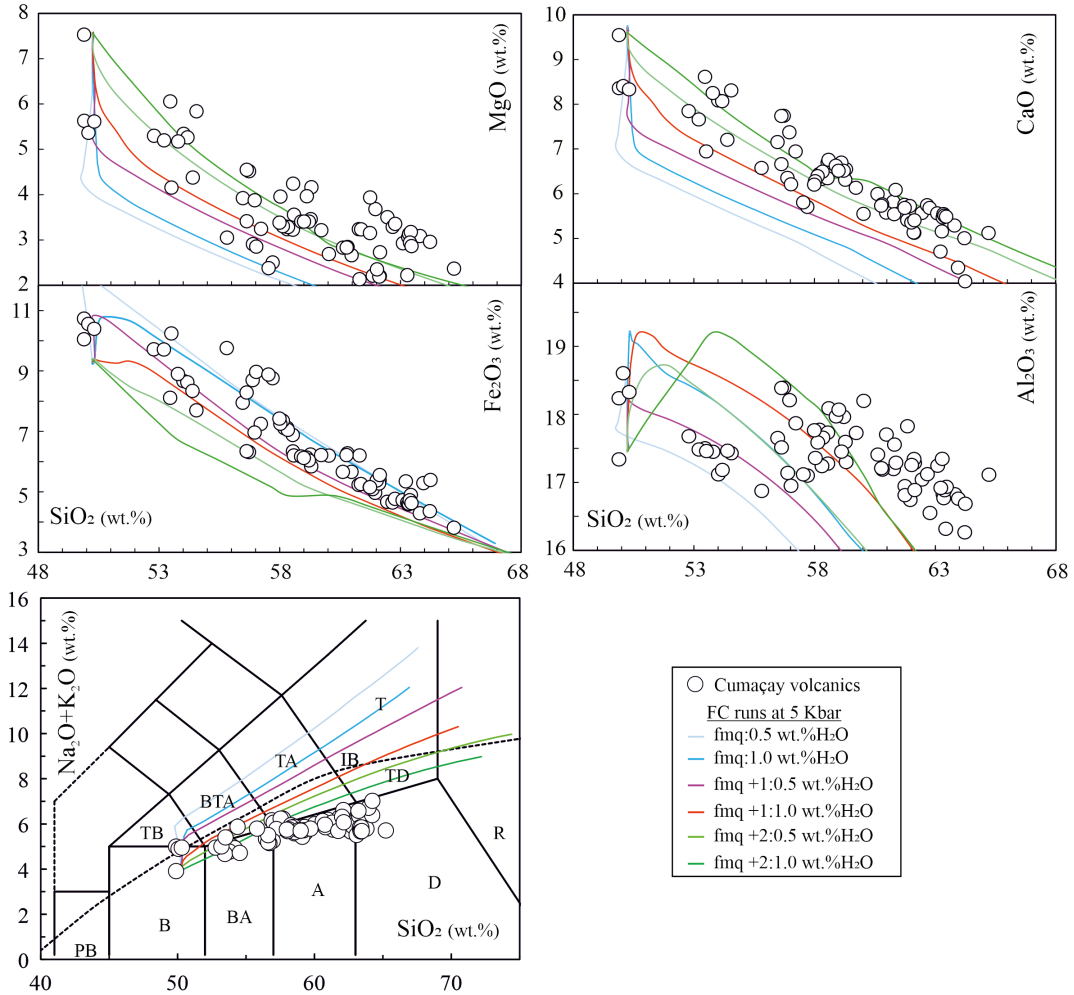

Figure 10. Fractional crystallization (FC) thermodynamic modeling results from Magma Chamber Simulator (MCS) software (Bohrson et al., 2014;2020) using the major element compositions of Cumaçay volcanics. Major elements are recalculated on an anhydrous basis.

and 25 mass unit. Compared to FC runs, AFC runs predict lower crystallinity ranging between approximately 74% and 54%. Crystallization phase assemblage is similar to the FC runs and composed of orthopyroxene (approximately 10–21 wt%), clinopyroxene (17–26 wt%), pigeonite (3–16 wt%), plagioclase (approximately 42–52 wt%), and Fe-Ti oxide (approximately 4–13 wt%). Apatite could not be stabilized in AFC runs. All major oxide contents of the modeled LLDs indicate higher values compared to the FC runs in a given SiO_2. The higher water contents do not have much effect on most of the major oxides; however, predicted higher Al_2O_3 contents depend upon the late crystallization of the plagioclase. Modeled curves at FMQ+1 and FMQ+2 with 1 wt% H_2O contents reproduce most of the basaltic, intermediate, and acidic members of Cumaçay for CaO, FeO, Al_2O_3, and to a lesser extent, MgO. Majority of Na_2O+K_2O contents of the Cumaçay volcanics ranging from basalts to dacites, replicated by FMQ+1 AFC run, which implies that the crustal contamination at mid to lower crustal depths could be responsible for the major element diversity of Cumaçay volcanics.

4.1.3. Recharge and fractional crystallization (RFC) model

The textural and compositional diversity of phenocrysts, wide distribution of calculated pressures and temperatures, and the existence of microcrystalline enclaves and crystal clots in andesites and dacites suggest magma mixing/recharge may be responsible for the generation of some of the evolved members of Cumaçay volcanics. Moreover, the linear trend and the mismatch between MCS-AFC curves and the Cumaçay whole rock data in the range of approximately 58–65 SiO_2 wt% and approximately 2.5–4 wt% MgO (Figure 11) also support this idea. To test the viability of mixing processes, we performed the RFC

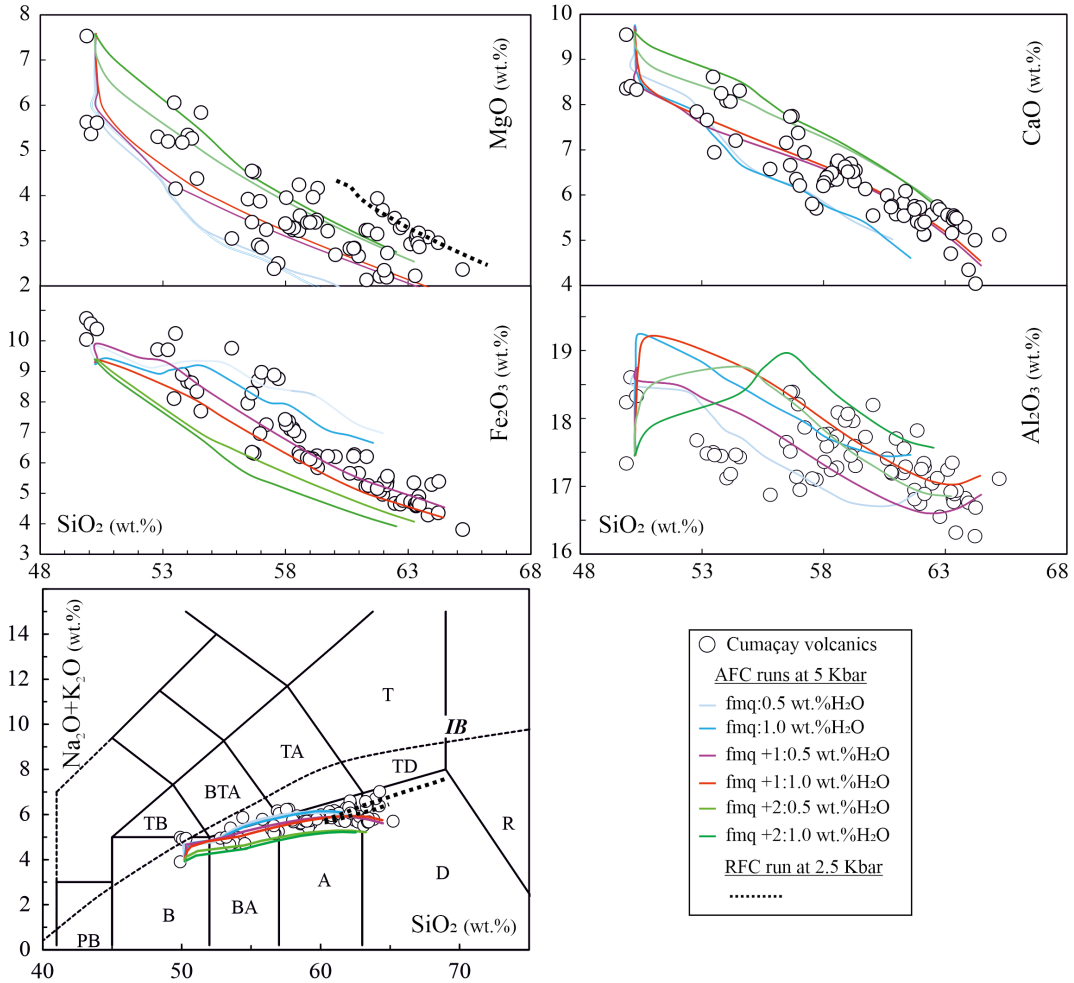

Figure 11. Assimilation and fractional crystallization (AFC) thermodynamic modeling results from Magma Chamber Simulator (MCS) software (Bohrson et al., 2014;2020) using the major element compositions of Cumaçay volcanics. Dotted lines in MgO and Na_2O+K_2O versus SiO_2 plots represent the recharge and fractional crystallization (RFC) modeling. See text for details. Major elements are recalculated on an anhydrous basis.

model using dacite (Cum238) for resident magma and a basaltic trachyandesite (Cum179) for recharge magma compositions (Table 2). The initial water concentrations of samples are in accordance with the plagioclase–liquid hygrometer for similar rock groups. The RFC model terminates 40 wt% of magma crystallization. The composition of solid cumulate is approximately 17 wt.% orthopyroxene, approximately 10 wt% clinopyroxene, approximately 61 wt% plagioclase, and approximately 12 wt% Fe-Ti oxide, which is similar to that FC and AFC runs. As demonstrated in Figure 11, the liquid line descent show suitable matches with the intermediate and acidic samples for MgO and the alkalis (Na_2O+K_2O) for comparable SiO_2 concentrations. In the MgO diagram, the andesitic and the dacidic samples that show linear tendency between approximately 58–65 SiO_2 wt% and approximately 2.5–4 wt% MgO contents correlate better with modeled liquid after the recharge event. Assimilation of country rocks may also incorporate shallow-level processes.

4.2. Magma plumbing system

Our observation from mineral thermobarometry and MCS runs let us have some limitations on the subvolcanic magma plumbing system under the Cumaçay. We suggest a two-stage petrogenetic model similar to that proposed for the Süphan volcano by Özdemir et al. (2011). In our model, mantle-derived basalt intrudes the lower to mid-crust (deep magma reservoir), where it disturbs the geothermal gradient forming a deep-crustal hot zone comparable to the model of Annen et al. (2006), which is suggested for arc environments. The surrounding crust undergoes partial melting when it exceeds the solidus and forms hybrid melt that includes remaining melts from the crystallization of the basalt and anatectic melt from the wall rock. AFC processes produce evolved melts that may contain various

differing SiO_2 content distributed across a wide depth range. It is challenging to constrain the precise depth range of the hot zone; however, thermobarometry results indicate a crystallization pressure range of approximately 4–8 kbar or 14–28 km. Additionally, geophysical studies suggest that the thickness of the crust in eastern Anatolia is in the range of 40–45 km (e.g., Özacar et al., 2010; Alkan et al., 2020) and have a low-velocity zone between 20 and 30 km (e.g., Angus et al., 2006; Karaoğlu et al., 2017; Zhu, 2018; Alkan, 2022), representing a partial melt pocket in the middle crust under the Late Cenozoic volcanic centers. The generated evolved melts migrate to shallow crustal levels, where they produce a subvolcanic magma reservoir. The crystallization pressures suggest around approximately 1.5–4.5 kbar or 5–15 km depth. Similar shallow magma storage regions have been reported for Plio-Quaternary (e.g., Karaoğlu et al., 2018) and Quaternary (e.g., Özdemir et al., 2011; Macdonald et al., 2015; Karaoğlu et al., 2017) volcanic centers in eastern Anatolia. The shallow magma storage region is where various melts come across and interact with each other. In addition to the wide range of calculated temperature/pressures and compositional variety of phenocrysts, the presence of crystal clots in andesite and dacite supply other evidence for the magma mixing (replenishment) process in a shallow magma reservoir. The plagioclase, pyroxene, and Fe-Ti oxide-bearing crystal clots in andesites and dacites indicate that they likely originated from the highly crystalline part (e.g., crystal mush) of the shallow reservoir. Injection of hot hybrid (or primitive) mafic magma into such reservoirs caused thermal erosion on crystal mushes (e.g., Neave et al., 2014; Zhang et al., 2015; Feng and Zhu, 2018). Finally, crystal clots can be formed by the disaggregation of those mushy zones (e.g., Feng and Zhu, 2018). The final chemical composition of intermediate and acidic magmas of Cumaçay volcanics would be the result of mixing between evolved (e.g., dacite) and basaltic (e.g., basalt; basaltic trachyandesite) melts.

5. Conclusion

Cumaçay consists of genetically related lava flows ranging in composition from basalt to dacite, representing one of the Plio-Quaternary eruption centers of postcollisional volcanism in Eastern Turkey. Our new K-Ar ages and whole rock geochemistry indicate that the volcanism started with the mildly alkaline basaltic lava flows (3.5 Ma), continued with subalkaline intermediate to acidic members (2.9–2.1 Ma), and ended up with transitional and subalkaline basaltic flows (2–0.97 Ma). Deep (approximately 14–28 km) and shallow (approximately 5–15 km) storage reservoirs have been recognized based on thermobarometric calculations beneath the Cumaçay. Our thermodynamic modeling using MCS reveals that the mantle-derived primitive magma intruded into the lower to the middle crust, where fractionation and crustal assimilation resulted in evolved melts with various SiO_2 contents. The generated evolved melts then migrate to shallow crustal levels, where they produce a subvolcanic magma reservoir. Petrographical observations, combined with whole-rock major element modeling, reveal that the evolved rocks (andesite and dacite) may be produced via combined processes of fractional crystallization, the interaction of colder (e.g., dacite) and hotter magmas (e.g., basalt; basaltic trachyandesite) ascending from depth and recycling of early formed crystals at shallow magma storage region.

Acknowledgments

This work has been funded by both Van-Yüzüncü Yıl University Scientific Research Project Foundation (2015-FBE-YL030) and TÜBİTAK, The Scientific and Technological Research Council of Turkey (Project No. 113Y406). We are grateful to S. Kearns for his help with the electron microprobe at Bristol. We warmly thank Orhan Karslı and two anonymous reviewers for helpful and constructive comments. We also thank Namık Aysal for editorial handling.

Supplementary Data

Supplementary data can be accessed at the following link: https://aperta.ulakbim.gov.tr/record/252343#.ZDfLRXZByUk

References

Açlan M, Altun Y (2018). Syn-collisional I-type Esenköy Pluton (Eastern Anatolia-Turkey): an indication for collision between Arabian and Eurasian plates. Journal of African Earth Sciences 142: 1-11.

Açlan M, Oyan V, Köse O (2020). Petrogenesis and the evolution of Pliocene Timar basalts in the east of Lake Van, Eastern Anatolia, Turkey: A consequence of the partial melting of a metasomatized spinel–rich lithospheric mantle source. Journal of African Earth Sciences 168: 103844. https://doi.org/10.1016/j.jafrearsci.2020.103844

Alkan H, Çınar H, Oreshin S (2020). Lake Van (Southeastern Turkey) experiment: receiver function analyses of lithospheric structure from teleseismic observations. Pure and Applied Geophysics 177 (8): 3891-3909.

Alkan H (2022). Crustal structure in and around the East Anatolian volcanic belt by using receiver functions stacking. Journal of African Earth Sciences 191: 104532.

Andersen DJ, Lindsley DH (1985). New (and final!) models for the Ti–magnetite/ilmenite geothermometer and oxygen barometer. In: Abstracts of American Geophysical Union 1985 Spring Meeting, American Geophysical Union 66 (18): 416.

Angus DA, Wilson DC, Sandvol E, Ni JF (2006). Lithospheric structure of the Arabian and Eurasian collision zone in eastern Turkey from S-wave receiver functions. Geophysical Journal International 166 (3): 1335-1346.

Annen C, Blundy J, Sparks RS (2006). The Genesis of Intermediate and Silicic Magmas in Deep Crustal Hot Zones. *Journal of Petrology 47*: 505-539.

Bacon CR, Hirschmann MM (1988). Mg/Mn partitioning as a test for equilibrium between Fe–Ti oxides. American Mineralogist 73: 57-61.

Bohrson WA, Spera FJ, Ghiorso MS, Brown GA, Creamer JB, Mayfield A (2014). Thermodynamic model for energy-constrained open-system evolution of crustal magma bodies undergoing simultaneous recharge, assimilation and crystallization: the magma chamber simulator. Journal of Petrology 55 (9): 1685-1717.

Bohrson WA, Spera FJ, Heinonen JS, Brown GA, Scruggs MA, Adams JV, Takach KM, Zeff G, Suikkanen E (2020). Diagnosing open-system magmatic processes using the Magma Chamber Simulator (MCS): part I—major elements and phase equilibria. Contributions to Mineralogy and Petrology 175 (11): 1-29.

Cashman KV, Sparks RSJ, Blundy JD (2017). Vertically extensive and unstable magmatic systems: a unified view of igneous processes. Science, 355 (6331): 1280. https://doi.org/10.1126/science.aag3055.

Ergen A, Sümengen M (2018). 1:100.000 ölçekli Ağrı İ50 Paftası. MTA Yayınları, Ankara.

Eskandari A, Amini S, De Rosa R, Donato P (2018). Nature of the magma storage system beneath the Damavand volcano (N. Iran): An integrated study. Lithos 300: 154-176. doi:10.1016/j.lithos.2017.12.002

Feng W, Zhu Y (2018). Decoding magma storage and pre-eruptive processes in the plumbing system beneath early Carboniferous arc volcanoes of southwestern Tianshan, Northwest China. Lithos 322: 362-375.

Ghiorso MS, Sack RO (1995). Chemical mass transfer in magmatic processes IV. A revised and internally consistent thermodynamic model for the interpolation and extrapolation of liquid-solid equilibria in magmatic systems at elevated temperatures and pressures. Contributions to Mineralogy and Petrology 119: 197-212. https://doi.org/ 10.1007/bf00307281

Ghiorso MS, Gualda GAR (2015). An H2O-CO2 mixed fluid saturation model compatible with rhyolite-MELTS. Contributions to Mineralogy and Petrology 169 (6): 1-30. https://doi.org/10.1007/s00410-015-1141-8

Gualda GAR, Ghiorso MS, Lemons RV, Carley TL (2012). Rhyolite-MELTS: a Modified Calibration of MELTS Optimized for Silica-rich, Fluid-bearing Magmatic Systems. Journal of Petrology 53 (5): 875-890. https://doi.org/10.1093/petrology/egr080

Gualda GAR, Ghiorso MS (2015). MELTS_Excel: a microsoft excelbased MELTS interface for research and teaching of magma properties and evolution. Geochemistry, Geophysics, Geosystems 16 (1): 315–324.

Irvine, TN, Baragar, WRA (1971). A Guide to the Chemical Classification of the Common Volcanic Rocks. Canadian Journal of Earth Sciences 8: 523–548.

Karaoğlu Ö, Özdemir Y, Tolluoğlu AÜ, Karabıyıkoğlu M, Köse O, Froger JL (2005). Stratigraphy of the volcanic products around Nemrut Caldera: Implications for reconstruction of the caldera formation. Turkish Journal of Earth Sciences 14: 123-143.

Karaoğlu Ö, Selçuk, AS, Gudmundsson A (2017). Tectonic controls on the Karlıova triple junction (Turkey): Implications for tectonic inversion and the initiation of volcanism. Tectonophysics 694: 368-384. doi.org/10.1016/j.tecto.2016.11.01800401951

Karaoğlu, Ö, Browning, J, Salah, MK, Elshaafi, A, Gudmundsson, A (2018). Depths of magma chambers at three volcanic provinces in the Karlıova region of Eastern Turkey. Bulletin of Volcanology 80 (9): 1-17.

Keskin M (1992a). Geochemical characteristics of collision related volcanism on the Erzurum-Kars plateau, northwestern Anatolia, Turkey. 29th International Geological Congress, Kyoto.

Keskin M, Pearce JA, Mitchell JG (1998). Volcano-stratigraphy and geochemistry of collision-related volcanism on the Erzurum-Kars Plateau, North Eastern Turkey. Journal of Volcanology and Geothermal Research 85: 355-404.

Keskin M (2003). Magma generation by slab steepening and breakoff beneath a subduction–accretion complex: An alternative model for collision-related volcanism in Eastern Anatolia Turkey. Geophysical Research Letters 30: 1-4.

Keskin M (2007). Eastern Anatolia: a hot spot in a collision zone without a mantle pluma In: Plates, Plumes and Planetary Processes. Special Papers Geological Society of America 430: 693-722.

Kıral K, Çağlayan A (1980). Kağızman (Kars)-Ağrı-Taşlıçay (Ağrı) dolayının jeolojisi: MTA Report (unpublished), Ankara.

Le Bas MJ, Le Maitre RN, Streckeisen A, Zanettin B (1986). A chemical classification of volcanic rock based on total silica diagram. Journal of Petrology 27: 745-750.

Lebedev VA, Sharkov EV, Keskin M, Oyan V (2010). Geochronology of Late Cenozoic volcanism in the area of Van Lake, Turkey: an example of development dynamics for magmatic processes. Doklady Earth Sciences 433 (2): 1031-1037.

Lebedev VA, Chugaev AV, Ünal E, Sharkov EV, Keskin M (2016). Late Pleistocene Tendürek Volcano (Eastern Anatolia, Turkey). II. Geochemistry and petrogenesis of the rocks. Petrology 24 (3): 234-270.

Lepage LD (2003) ILMAT: an excel worksheet for ilmenitemagnetite geothermometry and geobarometry. Computers Geosciences 29: 673–678.

Macdonald R, Sumita M, Schmincke HU, Bagiński B, White JC et al. (2015). Peralkaline felsic magmatism at the Nemrut volcano, Turkey: impact of volcanism on the evolution of Lake Van (Anatolia) IV. Contributions to Mineralogy and Petrology 169 (4): 1-22. https://doi.org/10.1007/s00410-015-1127-6

McNutt SR (2005). Volcanic seismology. Annual Review of Earth and Planetary Sciences 33: 461-491.

Neave DA, Maclennan J, Hartley ME, Edmonds M, Thordarson T (2014). Crystal storage and transfer in basaltic systems: the Skuggafjöll eruption, Iceland. Journal of Petrology 55 (12): 2311-2346.

Oyan V, Keskin M, Lebedev VA, Chugaev AV, Sharkov EV (2016). Magmatic evolution of the Early Pliocene Etrüsk stratovolcano, eastern Anatolian collision zone, Turkey. Lithos 256: 88-108. https://doi.org/10.1016/J.LITHOS.2016.03.017

Oyan V, Keskin M, Lebedev VA, Chugaev AV, Sharkov EV et al. (2017). Petrology and Geochemistry of the Quaternary Mafic Volcanism to the NE of Lake Van, Eastern Anatolian Collision Zone, Turkey. Journal of Petrology 58 (9): 1701-1728.

Oyan V (2018). Ar-Ar dating and petrogenesis of the Early Miocene Taşkapı-Mecitli (Erciş-Van) granitoid, Eastern Anatolia Collisional Zone, Turkey. Journal of Asian Earth Sciences 158: 210-226.

Özacar AA, Zandt G, Gilbert H, Beck SL (2010). Seismic images of crustal variations beneath the East Anatolian Plateau (Turkey) from teleseismic receiver functions. Geological Society, London, Special Publications 340 (1): 485-496.

Özdemir Y, Karaoğlu Ö, Tolluoğlu AÜ, Güleç N (2006). Volcanostratigraphy and petrogenesis of the Nemrut stratovolcano (East Anatolian High Plateau): the most recent post-collisional volcanism in Turkey. Chemical Geology 226 (3-4): 189-211.

Özdemir Y, Blundy JD, Güleç N (2011). The importance of fractional crystallization and magma mixing in controlling chemical differentiation at Süphan Stratovolcano, Eastern Anatolia, Turkey. Contributions to Mineralogy and Petrology 162: 573-597.

Özdemir Y, Güleç N (2014). Geological and geochemical evolution of the Quaternary Süphan Stratovolcano, Eastern Anatolia, Turkey: evidence for the lithosphere–asthenosphere interaction in post-collisional volcanism. Journal of Petrology 55 (1): 37-62. https://doi.org/10.1093/petrology/egt060

Özdemir Y, Akkaya I, Oyan V, Kelfoun K (2016) A debris avalanche at Süphan stratovolcano (Turkey) and implications for hazard evaluation. Bulletin of Volcanology 78: 9.

Özdemir Y, Mercan Ç, Oyan V, Özdemir AA (2019). Composition, pressure, and temperature of the mantle source region of quaternary nepheline-basanitic lavas in Bitlis Massif, Eastern Anatolia, Turkey: A consequence of melts from Arabian lithospheric mantle. Lithos 328: 115-129.

Özdemir Y, Oyan V, Jourdan F (2022). Petrogenesis of Middle Miocene to Early Quaternary basalts from the Karayazı–Göksu plateau (Eastern Anatolia, Turkey): Implication for the role of pyroxenite and lithospheric thickness. Lithos 416: 106671. https://doi.org/10.1016/j.lithos.2022.106671

Pearce JA, Bender JF, De Long SE, Kidd WSF, Low PJ et al. (1990). Genesis of collision volcanism in Eastern Anatolia, Turkey. Journal of Volcanology and Geothermal Research 44 (1-2): 189-229.

Polo LA, Giordano D, Janasi VDA, Guimarães LF (2018). Effusive silicic volcanism in the Paraná Magmatic Province, South Brazil: Physico-chemical conditions of storage and eruption and considerations on the rheological behavior during emplacement. Journal of Volcanology and Geothermal Research 355: 115-135.

Putirka KD (2005). Igneous thermometers and barometers based on plagioclase + liquid equilibria: Tests of some existing models and new calibrations. American Mineralogist 90: 336-346.

Putirka KD, Ryerson FJ, Mikaelian H (2003). New igneous thermobarometers for mafic and evolved lava compositions, based on clinopyroxene+liquid equilibria. American Mineralogist 88: 1542-1554.

Putirka KD (2008) Thermometers and barometers for volcanic systems. In: Minerals, Inclusions and Volcanic Processes. Mineralogical Society of America and Geochemical Society Reviews in Mineralogy and Geochemistry 69: 61-120.

Roeder PL, Emslie R (1970). Olivine-liquid equilibrium. Contributions to Mineralogy and Petrology 29 (4): 275-289. https://doi.org/10.1007/BF00371276

Sağlam Selçuk A, Mutlu S, Erturaç MK, Üner S, Sancar T et al. (2021). Balık Gölü Fay Zonu'nun Geometrisi ve Paleosismolojisi: Ön Bulgular, 24. Aktif Tektonik Araştırma Grubu Çalıştayı, İstanbul, Türkiye.

Spencer KJ, Lindsley DH (1981). A solution model for coexisting iron–titanium oxides. American Mineralogist 66 (11-12): 1189-1201.

Stormer JC (1983). The effects of recalculation on estimates of temperature and oxygen fugacity from analyses of multicomponent–iron–titanium oxides. American Mineralogist 68: 586-594.

Sun, SS, McDonough, WF (1989). Chemical and isotopic systematics of oceanic basalts: Implications for mantle composition and processes. In: Saunders, A.D.&Norry, M.J. (ed.) In Magmatism in Ocean Basins. Geological Society London Special Publication 42, 313-345.

Topuz G, Candan O, Zack T, Yılmaz A (2017). East Anatolian plateau constructed over a continental basement: No evidence for the East Anatolian accretionary complex. Geology 45 (9): 791-794.

Topuz G, Candan O, Wang JM, Li QL, Wu FY et al. (2021). Silurian A-type metaquartz-syenite to-granite in the Eastern Anatolia: Implications for Late Ordovician-Silurian rifting at the northern margin of Gondwana. Gondwana Research 91: 1-17.

Venezky DY, Rutherford MJ (1999). Petrology and Fe–Ti oxide reequilibration of the 1991 Mount Unzen mixed magma. Journal of Volcanology and Geothermal Research 89 (1-4): 213-230.

Waters LE, Lange RA (2015). An updated calibration of the plagioclase-liquid hygrometer-thermometer applicable to basalts through rhyolites. American Mineralogist 100 (10): 2172-2184. https://doi.org/10.2138/am-2015-5232

Weis D, Kieffer B, Maerschalk C, Barling J, de Jong J et al. (2006). High precision isotopic characterization of USGS reference materials by TIMS and MC-ICP-MS. Geochemistry, Geophysics, Geosystem 7. https://doi.org/10.1029/2006GC001283

White R, McCausland W (2016). Volcano-tectonic earthquakes: A new tool for estimating intrusive volumes and forecasting eruptions. Journal of Volcanology and Geothermal Research 309: 139-155.

Yılmaz Y, Güner Y, Şaroğlu, F (1998). Geology of the Quaternary volcanic centres of the East Anatolia. Journal of Volcanology and Geothermal Research 85 (1-4): 173-210.

Zhang J, Davidson JP, Humphreys MCS, Macpherson CG, Neill I (2015). Magmatic enclaves and andesitic lavas from Mt. Lamington, Papua New Guinea: implications for recycling of earlier-fractionated minerals through magma recharge. Journal of Petrology 56 (11): 2223-2256.

Zhu H (2018). High Vp/Vs ratio in the crust and uppermost mantle beneath volcanoes in the Central and Eastern Anatolia. Geophysical Journal International 214 (3): 2151-2163.